Nonlinear Poisson's Ratio for Modeling Hyperelastic Capacitive Sensors

Elze Porte and Rebecca Kramer-Bottiglio*

Highly stretchable capacitive sensors are of great interest for soft robotic control due to their ability to measure relatively large strains. These sensors are often multilayered materials, with one or more of the layers made from silicones filled with functional particles. However, the models used to describe the material behavior do not always account for the hyperelastic nature of the silicones, the altered material properties due to fillers, and potential anisotropy due to the layered structure. Large errors arise when predicting capacitance using widespread assumptions of linear elastic mechanics and isotropic material properties. This study demonstrates how these modeling assumptions are inadequate for predicting sensor performance, and compares alternative models based on empirical material mechanics. The Poisson's ratio of multi-layered hyperelastic capacitors is measured in both the width and thickness directions by imaging the sensor dimensions during strain. The results indicate that the sensors are anisotropic and have a strain-dependent Poisson's ratio, demonstrating the validity of the proposed model. Considering these properties in capacitance models will lead to an improved ability to predict sensor performance, especially at high strains.

1. Introduction

Elastomeric capacitive strain sensors are a promising technology to measure the large strains associated with soft robotic systems. They have been used for closed-loop control[1–5] and exhibit consistent performance over thousands of strain cycles.[6–8] Current sensor models are inadequate for predicting electromechanical performance due to two fundamental deficiencies. First, the sensors are often made from hyperelastic silicones, but most models are based on linear elastic mechanics.[8–14] Second, the conductive layers added to the silicone to create electrodes have different properties than neat silicone, and can significantly affect the overall material properties of the sensor.[6,9] To advance capacitive sensor design and improve integration with soft robotic systems, a greater understanding of the nonlinear mechanics and the influence of the conductive layers on capacitive sensor performance is required. In this work, we demonstrate that accounting

for nonlinear and anisotropic material properties improves our prediction of capacitance by at least 15% compared to models based on traditional assumptions.

Capacitive sensors measure strain based on changes in the geometry of the sensor during stretch. A very common sensor design is the parallel-plate capacitor,[6,7,10,15–17] where thin electrode and dielectric layers are stacked. For ideal plate capacitors, the capacitance C is related to the sensor dimensions by

$$C = \epsilon_0 \, \epsilon_r \, \frac{Lw}{t} \tag{1}$$

where ϵ_0 and ϵ_r are the free space and relative permittivity, respectively; L and w are the length and width of the active area of the sensor, respectively; and t is the thickness of the dielectric layer. The dimensions of the sensor change during stretch, resulting in a measurable change in capacitance. The changes in the different dimensions of the sensor are related by the Poisson's ratio v, as schematically shown in 2D in **Figure 1**a. When the Poisson's ratio of the sensor is known, the capacitance can be predicted for any change in L by expressing w and t as a function of the strain in length direction ε_L.

The layered structure and the different material properties of electrodes and dielectric materials should be considered when describing the Poisson's ratio. Electrode layers can be made from a composite of elastomer and conductive filler, such as graphite[1,6] or carbon black.[7,15,18] The addition of fillers generally reduces the Poisson's ratio of the composite compared to neat silicone[19–22] due to a mismatch between the Poisson's ratio of the elastomer and of the filler material.[19,23] Similarly, a mismatch between the Poisson's ratio of the electrode and the dielectric layers is expected to result in a Poisson's ratio of the sensor as a whole in between those of the separate layers.[24] In addition, fillers in the silicone matrix can result in a strain-dependent Poisson's ratio.[19,21,25,26] Nonlinear capacitance models for pressure sensors highlight the importance of accurate material assumptions,[27,28] but, to the authors' knowledge, no study provides empirical evidence for a nonlinear capacitance model for stretch sensors, and there are no studies investigating the potential strain-dependent Poisson's ratio of capacitive sensors.

The aim of this study is to use empirical material mechanics to develop a hyperelastic capacitance model that accurately predicts the measured capacitance at large strains. We use silicone (DragonSkin10, Smooth-on, Inc) based sensors with expanded

Dr. E. Porte, Prof. R. Kramer-Bottiglio
Department of Mechanical Engineering and Materials Science
9 Hillhouse Av
New Haven, CT 06511, USA
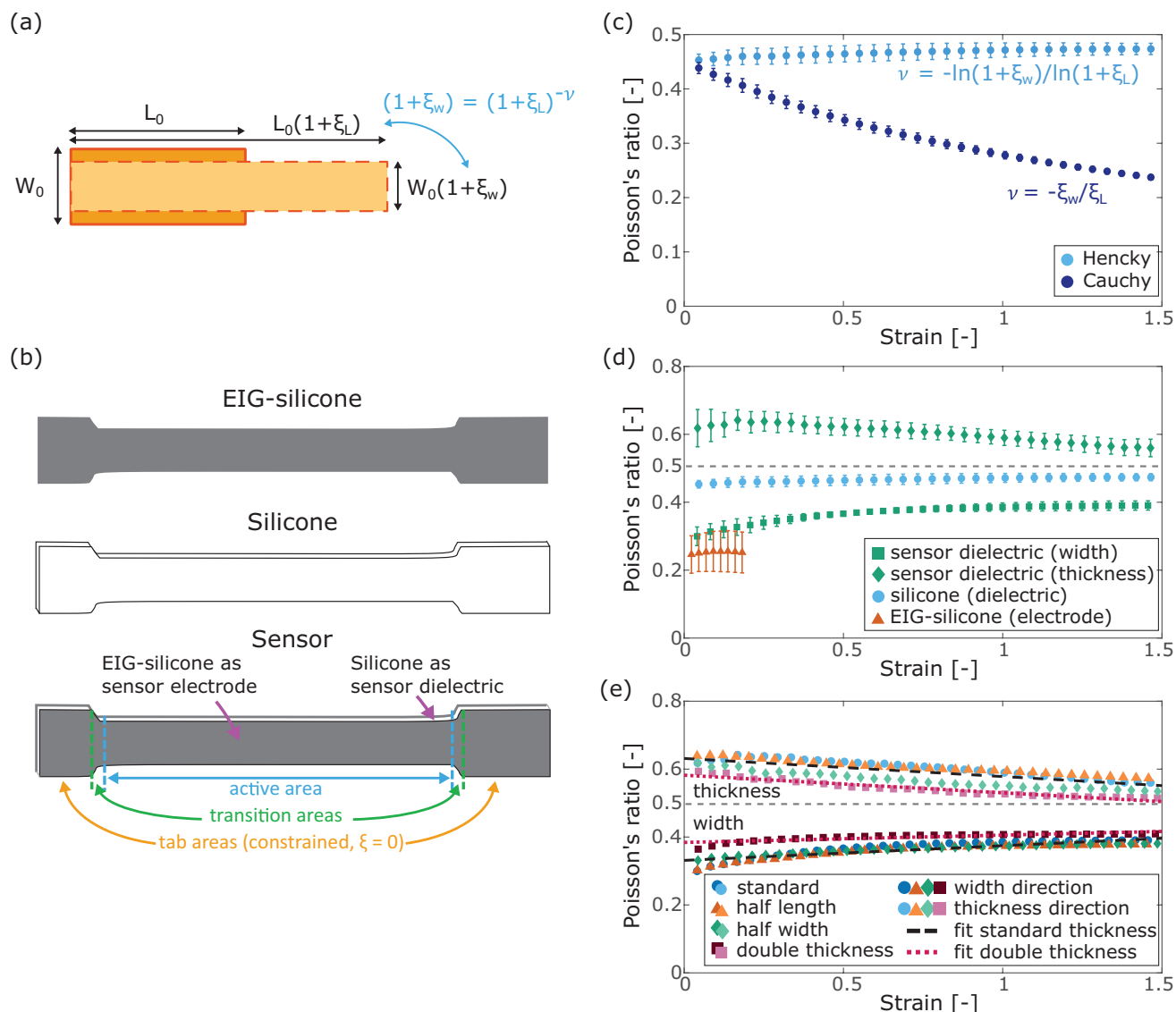E-mail: rebecca.kramer@yale.edu

Figure 1. a) Schematic representation of Poisson's ratio; b) schematic representation of the individual layers and sensor layout; c) comparison of Poisson's ratios of linear and hyperelastic models; d) Poisson's ratios of the individual layers of the sensor, and the dielectric as part of the sensor; e) Poisson's ratios of different sensor geometries including a linear fit to the data. The incompressibility condition ($\nu = 0.5$) is indicated with a black dotted line in (d) and (e) ($n = 6$ for all).

intercalated graphite (EIG)–silicone electrodes, as described in previous work,[1,6] and schematically represented in Figure 1b. First, we analyzed the Poisson's ratio of silicone, comparing a linear elastic and hyperelastic model. Second, we investigate the Poisson's ratio of the individual layers of the sensor, and as a complete sensor structure for different sensor dimensions. Variations in the sensor dimensions are all compared to our "standard" sensor, which has an initial active sensor area of 100×10 mm and dielectric thickness of approximately 0.6 mm. Dimensions of all sensor geometries are given in Table S1 in the Supporting Information. Third, we translated the measured Poisson's ratio into a prediction of capacitance and compared the use of different models to the measured capacitance. Fourth, we predict the capacitance of sensors without direct measurements of Poisson's ratio, but based on the empirical model.

2. Results and Discussion

There are two primary definitions of Poisson's ratio: Cauchy's linear elastic ratio and Hencky's hyperelastic ratio.[25] The definition of the linear elastic Poisson's ratio is

$$\nu_w = -\varepsilon_w/\varepsilon_L \tag{2}$$

whereas the hyperelastic Poisson's ratio is

$$\nu_w = -\ln(1+\varepsilon_w)/\ln(1+\varepsilon_L) \tag{3}$$

with ν_w being the Poisson's ratio in width direction, and ε_w and ε_L the strains in width and length direction, respectively. Replacing ε_w in Equations (2) and (3) with the strain in thickness direction

**ADVANCED
SCIENCE NEWS**
www.advancedsciencenews.com

**ADVANCED
MATERIALS
TECHNOLOGIES**
www.advmattechnol.de

ε_t results in the Poisson's ratio in thickness direction ν_t. Figure 1c compares the two definitions by showing the linear and hyperelastic ν_w for silicone up to 150% strain. The hyperelastic analysis results in a constant ν_w close to 0.5, while the linear elastic model results in a strongly decreasing ν_w. The observed difference between the two models is in line with the literature on hyperelastic behavior of elastomers.[25,29] Unless otherwise stated, we will use the hyperelastic definition of Poisson's ratio so the near incompressibility of the silicone can be expressed as $\nu_w + \nu_t \approx 1$.

The Poisson's ratio of the EIG–silicone, silicone, and silicone as sensor dielectric (Figure 1b) were measured to investigate the isotropy and strain dependence of the sensor. Figure 1d shows ν_w and ν_t over 150% strain for the sensor dielectric, and ν_w for the individual layers, which are expected to be isotropic ($\nu_w = \nu_t$). The EIG–silicone failed at strains higher than 20%. We found that the Poisson's ratio of the sensor dielectric is lower in width direction (≈0.30–0.39) than in thickness direction (≈0.56–0.62), and changes with strain in both directions. The following paragraphs will first discuss the directionality of the sensor and subsequently the strain dependence.

The reduction of Poisson's ratio of the sensor in the width direction can be explained by the mismatch of the Poisson's ratios of the dielectric and electrode materials: the Poisson's ratio of the EIG-silicone (≈0.25) is much lower than the pure silicone (≈0.47) when tested separately (Figure 1d). The mismatch of Poisson's ratios results in ν_w of the sensor dielectric in between those of the individual layers (≈0.30–0.39), whereas ν_t (≈0.56–0.64) increases because the dielectric is a nearly incompressible material, where in this case $\nu_w + \nu_t \approx 0.94$. Other studies have reported a similar reduction in Poisson's ratio due to the addition of strain limiting[6,9] or auxetic layers to the sensor.[8,30] The difference between the Poisson's ratio in width and thickness directions means the sensor cannot be assumed isotropic. Although nonlinear mechanics models (e.g., Neo-Hookean, Ogden) can be fit to the stress–strain curves, these models do not capture the anisotropic nature of the sensors and are therefore not suitable as sensor models.

A similar observation was made regarding the stiffness of the sensors; The EIG-silicone is much stiffer (≈0.8 MPa secant modulus over 10% strain) than the dielectric silicone (≈0.2 MPa secant modulus over 10% strain), resulting in a modulus of the sensor as a whole in between those of the individual layers (≈0.3 MPa secant modulus over 10% strain). The average stress–strain curves for the EIG-silicone, silicone, and sensor are included in Figure S1 in the Supporting Information. The stiffness of the sensors can affect the overall stiffness of a soft robotic system and should therefore be considered in the system design, but the measured capacitance is not dependent on the sensor stiffness (Equation (1)).

The Poisson's ratio of the sensor's dielectric was not constant with strain (Figure 1d): ν_w increased from approximately 0.30 at 0% strain to 0.39 at 150% strain, and ν_t decreased from approximately 0.62 to 0.56 over the same strain interval. A strain-dependent Poisson's ratio has been reported for sensors that include auxetic structures,[11] but has not been investigated for capacitive sensors in general. The addition of the electrodes introduced a compressible component to the sensor, which likely affected the overall material behavior and resulted in a strain-dependent Poisson's ratio.

The anisotropic, strain dependent behavior was observed for all tested sensors geometries. Figure 1e shows the average measured Poisson's ratio over strain and a linear fit of the data in both width and thickness direction for three additional sensor designs: a "half-length," "half-width," and "double thickness" sensor. The results from the standard sensor are repeated from Figure 1d to provide a clear comparison. The standard deviations of the measurements are not shown for clarity, but are included in Figure S2 in the Supporting Information.

The measurements of the standard, half-width, and half-length sensors show almost identical Poisson's ratios. The half-width sensor shows a slightly lower average ν_t compared to the standard and half-length sensors, which we hypothesize is due to the sensitivity of the measurement method in thickness to small vibrations and twists in the sample that are more prone to appear in the smaller samples. As a result, both the half-length and half-width sensors showed a much larger range in the measured ν_t compared to the other sensors. The Poisson's ratio is assumed to be the same for sensors with the same thickness, since ν_w was identical for all sensors with the same dielectric thickness, and the small reduction in ν_t for the half-width sensor likely resulted from the sensitivity in the experimental method.

The potential effect of unwanted twisting in the sensor on the measured capacitance was further investigated by stretching the sensors in a twisted state, with the top end of the sample rotated 90° with respect to the bottom. We did not observe any differences between the measured capacitance of the twisted and straight sensors (measurements are included in Figure S3 in the Supporting Information). Small twisting motions of the sensors are therefore not further accounted for in the current work. In general, we expect the additional strains and the associated change in capacitance that result from a twisting motion to be relatively small in sensors with a much larger length than their width and thickness.

The double thickness sensor shows a slightly higher ν_w and lower ν_t compared to the other sensors. Qualitatively, this is line with the composite rule of mixtures, which predicts the Poisson's ratio of a composite material ν_{comp} based on the volume ratio φ of the materials ($\nu_{comp} = \nu_1\varphi_1 + \nu_2\varphi_2$).[31–33] Because the dimensions of the dielectric and electric layers are the same in length and width, only the thickness of the layers affects the volume ratio. The rule of mixtures, however, is based on linear elastic assumptions and assumes isotropy, and did therefore not provide a quantitative prediction of the Poisson's ratios that matched the experimental data for the sensor composites.

The insights into the Poisson's ratio of the sensor can be used to translate the material properties into an accurate capacitance prediction. Several capacitance models are considered in predicting the measured capacitance of the sensors. The most commonly used model assumes linear solid mechanics[8–14,18]

$$C = C_0 \frac{(1+\varepsilon_L)(1-\nu_w\varepsilon_L)}{(1-\nu_t\varepsilon_L)} \tag{4}$$

with C_0 being the initial capacitance at 0% strain. Taking into account the nonlinear mechanics and the anisotropy, while

keeping the assumption on the incompressibility of the dielectric layer, the capacitance–strain relationship is predicted by[6,7]

$$C = C_0 \frac{(1+\varepsilon_L)(1+\varepsilon_L)^{-v_w}}{(1+\varepsilon_L)^{-v_t}} = C_0 (1+\varepsilon_L)^{2(1-v_w)} \quad (5)$$

When the sensor is assumed as an isotropic incompressible material ($v_w = v_t = 0.5$),[7,9,10,12–14,17] both the linear- and hyperelastic models reduce to

$$C = C_0 (1+\varepsilon_L) \quad (6)$$

Using the strain-dependent empirical data on v_w and v_t in Equation (5) results in the empirical model presented in this study.

It is well documented that capacitance and strain are linearly related for elastomeric capacitive sensors.[6,7,10,15] At high strains, inaccurate measurements of the capacitance may occur due to an increasing resistance in the electrodes in combination with the chosen measurement frequency,[15,34] resulting in

a seemingly nonlinear relationship. The nonlinearity is, however, a measurement artifact, and if it occurred in the current work the linear part of the data was extrapolated to 150%. The measured Poisson's ratios at 5% strain were used as constant v_w and v_t in the theoretical models.

Figure 2a shows the linear fit (extrapolated from 100%) of the standard sensor compared to the predictions based on the models from Equations (4)–(6) and the empirical model based on the measured Poisson's ratio. The only model that accurately predicts the capacitance at 150% strain is the empirical model. The assumption of an isotropic incompressible material underestimates the capacitance by almost 15% at 150% strain, overestimating the strain by about 30%. Similarly, the incompressible hyperelastic model with constant strain underestimates the strain by about 30%. Although the linear elastic model performs similarly to the other models up to about 30% strain, it overestimates the capacitance at large strains, because the strain dependent Poisson's ratio (Figure 1c) was not accounted for. It is therefore essential to consider the strain-dependent Poisson's ratio for an accurate prediction of the capacitance.
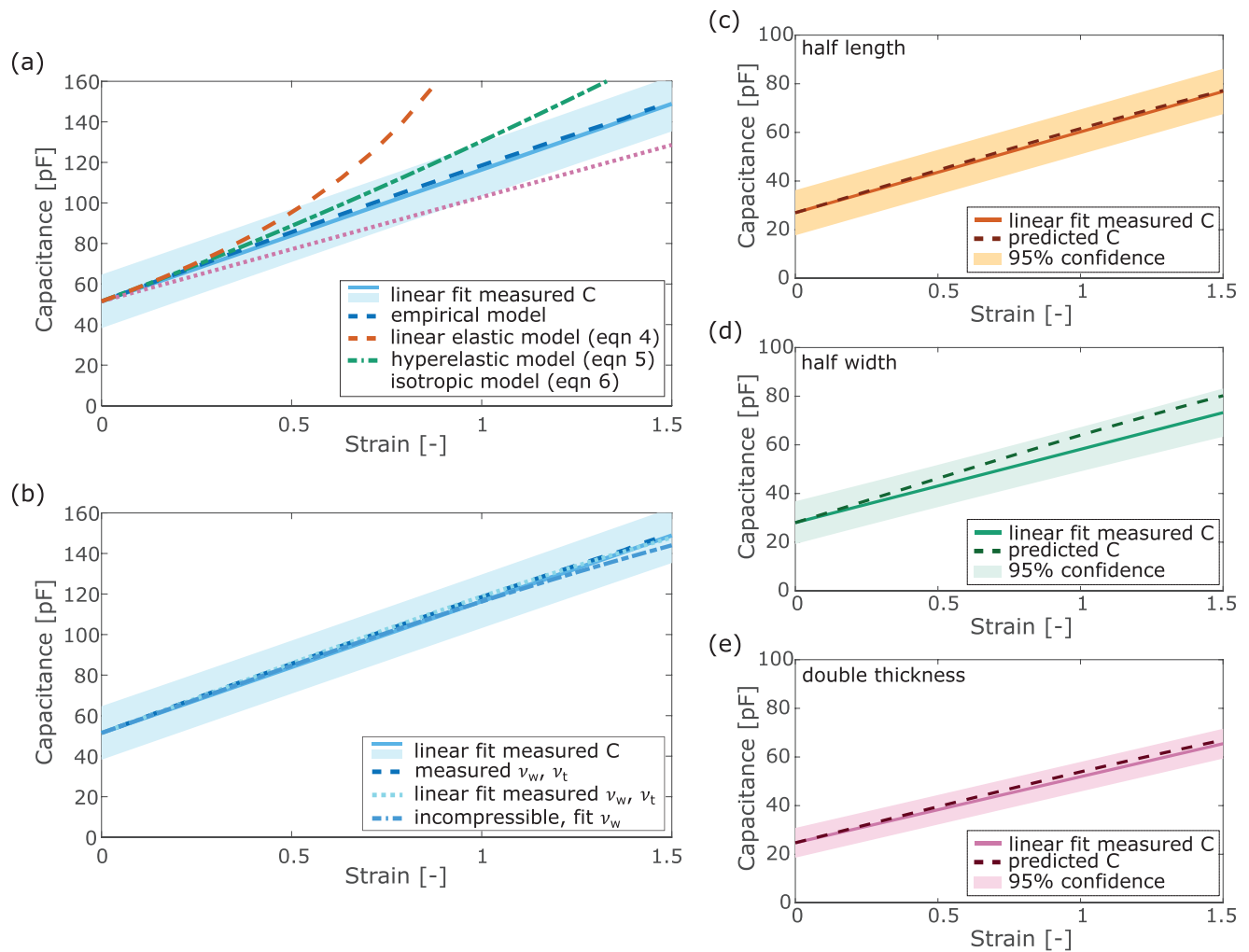

Figure 2. a) Predicted capacitance based on different models compared to the measured capacitance. The light blue shaded area indicates the 95% confidence interval of the linear fit to the experimental capacitance data. b) Comparison of different empirical models. Predicted capacitance using a linear fit to Poisson's data for c) half-length, d), half-width, and e) double thickness sensors ($n = 6$ for all).

The empirical model was further refined by predicting the capacitance based on a linear fit of the measured Poisson's ratio, and by assuming near incompressibility of the dielectric ($v_w + v_t = 0.94$) where the fit of v_w was used to calculate v_t. The comparison of these models, shown in Figure 2b, indicates that all models provide a close prediction of the capacitance. Although the models that use both the measurements of v_w and v_t are slightly more accurate, assuming incompressibility can save valuable testing and analysis time. This final empirical model can accurately predict the electromechanical performance of the different sensor variations (Figure 2c–e). Although the prediction for the half-width sensor (Figure 2d) deviates more from the measured capacitance than is the case for the half-length and double thickness (Figure 2c,e), the prediction still falls within the confidence interval. As expected from Equation (1), the reduction in length and width and increase in thickness for the sensor variations resulted in an almost identical C_0 (24–30 pF) at 0% strain that is about half C_0 of the standard sensor (50 pF). The double thickness sensor (Figure 2e) has a slightly lower capacitance increase per unit strain than the other sensors, which can be related to its different Poisson's ratio.

The Gauge factor (($\Delta C/C$)/($\Delta L/L$)) is larger than 1 for all sensor variations. For isotropic sensors with a nearly incompressible dielectric material ($v \approx 0.5$) the Gauge factor will not exceed 1.[7,10] The increased sensitivity of the sensors in the current work is a direct consequence of the low Poisson's ratio of the electrodes, since a low Poisson's ratio in width direction and high Poisson's ratio in thickness direction of the dielectric increases the capacitance change per unit strain (Equation (5)). The Poisson's ratio mismatch between the sensor layers can be exploited to increase sensor sensitivity by adding materials with a low Poisson's ratio to the composite structure, such as auxetic materials[8,30] and fabrics.[9] The Poisson's ratio of particle filled composites can generally be reduced by increasing the filler content,[19,20,22,26] but there may be practical limits since we observed embrittlement of the conductive composite in previous work that used a high filler content (>15 wt%).[35]

The empirical Poisson's ratio model was used to predict the sensor performance without directly measuring Poisson's ratio. Two additional sensor designs were chosen: sensors with approximately half the dielectric thickness of the standard sensor to investigate if the model can be extrapolated for thin dielectrics; and sensors that are a quarter the length and half the width of the standard sensor to check if the model is accurate for much smaller active areas that deviate from the standard sensor in more than one direction. The graphs in **Figure 3** show that, for both sensors, the predicted capacitance closely matches the experimental capacitance data.

The prediction of the quarter length sensors (Figure 3a) can be improved by accounting for the deformations in the transition area between the gauge aura with uniform strain and the tab area with no strain (as defined in Figure 1b). In all sensors, the strain was assumed uniform across both the transition and gauge area, since the transition area accounted for only a small percentage of the total stretchable area (<10%). In the small sensors, the transition area is larger than 20%, and assuming that the average strain in this area is 0.5 times the strain in the gauge area provided an even closer prediction of the measured capacitance (adapted model is included in the Supporting Information).
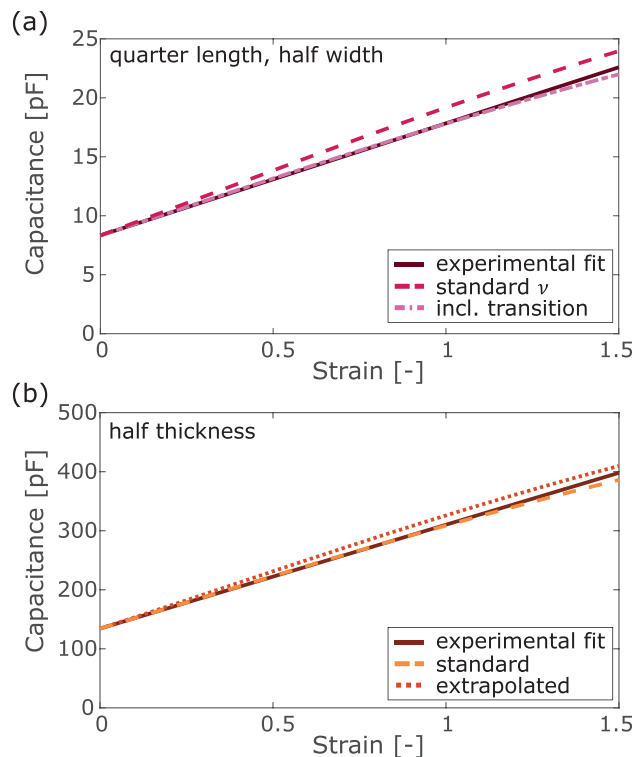

Figure 3. Predictions of capacitance without direct measurements of Poisson's ratio for a) a quarter length, half-width sensor based on the standard model and accounting for the transition area (Figure 1b) of the sensor, and b) a half-thickness sensor based on the standard model and on an extrapolated model accounting for layer thickness ($n = 4$ for all).

For the half-thickness sensors (Figure 3b), the capacitance was predicted using both the Poisson's ratio of the standard thickness sensors and an extrapolated Poisson's ratio to account for the reduction in dielectric thickness (the extrapolated Poisson's ratio calculation is included in the Supporting Information). Both predictions show close correspondence to the experimental data, and the difference between the two predictions is much smaller than between different models as presented in Figure 2a. The half-thickness sensors were the only samples where we observed buckling in the lateral direction when tensile strain was applied. Since the model provided accurate predictions of the capacitance, we did not include potential buckling effects in the model. Considering the strain-dependent hyperelastic Poisson's ratio is more important than accounting for small variations due to sensor thickness.

Studies that directly compare a capacitance model to measured data show either over- or underestimates of predicted capacitance.[10,12] The comparison of the different models in the current work indicates that it is essential to include the hyperelastic nature of the sensors to accurately predict their capacitance at high strains. Isotropic sensors are an exception to this, since the hyperelastic and elastic models are identical. Although some capacitive sensors with extremely thin electrodes may be assumed isotropic,[10] the assumption should be carefully considered due to the Poisson's mismatch between the conductive and dielectric layers.

The presented model is the first step to predict the Poisson's ratio of the sensor composite based on the Poisson's ratio of the individual layers. Currently, the model relies on the collected empirical data specific to the sensors. Hyperelastic material models, such as Neo-Hookean and Ogden assume isotropy, and can therefore not be directly used to model the mechanics of the sensors. Traditional composite models such as Voigt and Reuss have been reported to be insufficient to describe nonlinear material mechanics for fiber and particle composites,[36,37] and for materials with an incompressible matrix.[38] Although adapted composite models are presented in literature,[20,38] the experimental verification for a generalized theory is limited. Further understanding of the material mechanics of hyperelastic composite materials is required to accurately predict the Poisson's ratio of the sensor composite.

3. Conclusion

This work investigated the nonlinear and strain dependent material properties of elastic capacitive sensors by using a measured Poisson's ratio to predict sensor capacitance. The presented empirical model contributes to our understanding of hyperelastic capacitive sensors and can be used in the sensor design process to predict sensor sensitivity. Two main conclusions can be drawn. First, considering hyperelastic and anisotropic properties of the sensor is essential to accurately predict capacitance. The presented model showed much higher accuracy than models based on linear elastic and isotropic assumptions. Anisotropy was caused by a mismatch in the Poisson's ratio of the dielectric and electrode layers of the sensor. Second, the capacitance was most accurately predicted when the strain dependence of the Poisson's ratio was considered. The sensors showed an increasing Poisson's ratio in width direction, and decreasing Poisson's ratio in thickness direction with strain. The capacitance was also accurately described for sensors of which the Poisson's ratio was not directly measured, but the strain-dependence of the Poisson's ratio was included in the description.

4. Experimental Section

Dielectric Silicone: DragonSkin10 Slow (Smooth-on, Inc) was dyed white for imaging purposes using Silc Pig (Smooth-on, Inc) silicone dye. Part A was mixed with approximately 6 wt% white dye and stirred manually to ensure even distribution of the dye in the final product. Part B was added in equal ratio to the dyed Part A, and mixed in a centrifugal mixer (Thinky ARE-310) at 2000 rpm for 30 s and degassed at 2200 rpm for 30 s.

Conductive Composite Silicone: Expanded intercalated graphite (EIG) was prepared as conductive filler to DragonSkin10 Fast (Smooth-on, Inc) for the electrode layers of the sensors. Expandable graphite (5 g, Sigma Aldrich) was expanded in a crucible heated to 800 °C, and subsequently soaked in cyclohexane (500 mL). The mixture was sonicated (Q500 1/2″ tip, Qsonica) at 70% for 1 h and sieved through a 212 μm sieve. Excess cyclohexane was decanted after settling of EIG particles for at least 1 h, and the mixture was boiled down until approximately 3 wt% EIG was achieved. Silicone was prepared with equal Parts A and B and mixed as described for the dielectric silicone. The EIG mixture was manually stirred into the silicone at 79 wt% to achieve approximately 10 wt% EIG in the electrodes after evaporation of the cyclohexane during curing.

Sensor Fabrication: Sensors were produced using an earlier reported method.[6] The conductive EIG-silicone composite was rod-coated with a thickness of approximately 0.2 mm on a PET substrate. After curing, the dielectric silicone was coated on top of the EIG layer using a film applicator (SH0340, TQC Sheen), and the resulting sheet was folded onto itself just before full curing. The applicator settings were 450, 750, and 1350 μm for the half-thickness, standard thickness, and double thickness sensors, respectively. The final thickness is slightly lower than the coated thickness due to slight spreading of the silicone before curing. Sensors were cut to size with a laser cutter (VLS 2.30, Universal Laser Systems).

Sensor Interfacing: The sensors were interfaced with an LCR meter (E4980AL, Keysight Technologies) using copper strips glued to the sensor tabs (Figure 1b). Conductive glue was prepared by mixing Silpoxy (Smooth-On, Inc.) with the EIG mixture in the same ratio as the electrode layers. The copper strips were attached to a tab that was stationary during mechanical testing. Custom made attachments were glued with Silpoxy to either side of the sensor tabs to securely attach the sensors to the materials testing system.

Precycling Sensors: Samples were repeatedly (10×) stretched using a material testing system (Instron 3345) to 200% their original length before electromechanical testing to exclude the Mullin's effect from the measurements. The length of the stretchable area of the samples after the cyclic test was recorded as the new original length (L_0).

Electromechanical Characterization: Sensors were stretched to approximately 150% strain from L_0, at a rate of 5 mm s^{-1} using the materials testing system. For the half-length sensors, the rate was reduced to 2.5 mm s^{-1}. The capacitance of the sensors was recorded with the LCR meter at an excitation frequency of 400 Hz. Simultaneously, either the sensor width or thickness were captured with an imaging system (Grasshopper 3, Point Grey Research). Images were captured at approximately every 5% strain. The measured capacitance was adjusted to represent only the capacitance of the stretchable area by subtracting the capacitance of the stationary tab areas (Figure 1b) from the LCR measurements. The capacitance of the tab areas was calculated as a percentage of the initial capacitance C_0 using the relative size of the tab areas reported in Table S1 in the Supporting Information.

Image Analysis: Images were analyzed using the contrast of the black EIG layer against a white background for the width measurements and using the contrast between the white dielectric and black EIG layers for the thickness measurements. The width of the sensor was found by taking the average width over a length of 40–45 mm for each image. The thickness evolution of the dielectric was found by tracking the thickness change of a specified area over two subsequent images. This more detailed tracking method was required for the thickness measurements, due to the relatively large variation in thickness compared to the variation in width across the sensor.

Supporting Information

Supporting Information is available from the Wiley Online Library or from the author.

Acknowledgements

Conflict of interest

The authors declare no conflict of interest.

[1] M. C. Yuen, T. R. Lear, H. Tonoyan, M. Telleria, R. Kramer-Bottiglio, *IEEE Robot. Autom. Lett.* **2018**, *3*, 1402.

[2] B. K. Johnson, V. Sundaram, M. Naris, E. Acome, K. Ly, N. Correll, C. Keplinger, J. S. Humbert, M. E. Rentschler, *IEEE Robot. Autom. Lett.* **2020**, *5*, 3783.

[3] R. Zhang, P. Iravani, P. Keogh, *Sen. Actuators, A* **2017**, *264*, 123.

[4] S. Rosset, B. M. O'Brien, T. Gisby, D. Xu, H. R. Shea, I. A. Anderson, *Smart Mater. Struct.* **2013**, *22*, 104018.

[5] R. Agarwal, S. Bergbreiter, *IEEE Int. Conf. Soft Robot.* **2019**, 330.

[6] E. L. White, M. C. Yuen, J. C. Case, R. K. Kramer, *Adv. Mater. Technol.* **2017**, *2*, 1700072.

[7] J. Shintake, E. Piskarev, S. H. Jeong, D. Floreano, *Adv. Mater. Technol.* **2018**, *3*, 1700284.

[8] J. Shintake, T. Nagai, K. Ogishima, *Front. Robot. AI* **2019**, *6*, 127.

[9] A. Atalay, V. Sanchez, O. Atalay, D. M. Vogt, F. Haufe, R. J. Wood, C. J. Walsh, *Adv. Mater. Technol.* **2017**, *2*, 1700136.

[10] O. Atalay, A. Atalay, J. Gafford, H. Wang, R. Wood, C. Walsh, *Adv. Mater. Technol.* **2017**, *2*, 1700081.

[11] Y. J. Lee, S. M. Lim, S. M. Yi, J. H. Lee, S. G. Kang, G. M. Choi, H. N. Han, J. Y. Sun, I. S. Choi, Y. C. Joo, *Extreme Mech. Lett.* **2019**, *31*, 100516.

[12] D. J. Cohen, D. Mitra, K. Peterson, M. M. Maharbiz, *Nano Lett.* **2012**, *12*, 1821.

[13] H. S. Shin, A. Charalambides, I. Penskiy, S. Bergbreiter, *IEEE Int. Conf. Intell. Robot. Syst.* **2016**, 5572.

[14] M. Amjadi, K. U. Kyung, I. Park, M. Sitti, *Adv. Funct. Mater.* **2016**, *26*, 1678.

[15] A. Tairych, I. A. Anderson, *Soft Robot.* **2019**, *6*, 389.

[16] R. P. Rocha, P. A. Lopes, A. T. de Almeida, M. Tavakoli, C. Majidi, *J. Micromech. Microeng.* **2018**, *28*, 034001.

[17] S. Yao, Y. Zhu, *Nanoscale* **2014**, *6*, 2345.

[18] V. Tsouti, V. Mitrakos, P. Broutas, S. Chatzandroulis, *IEEE Sens. J.* **2016**, *16*, 3059.

[19] S. M. Smith, D. S. Simmons, *Soft Matter* **2019**, *15*, 656.

[20] W. Wu, K. Sadeghipour, K. Boberick, G. Baran, *Mater. Sci. Eng., A* **2002**, *332*, 362.

[21] C. G. Robertson, R. Bogoslovov, C. M. Roland, *Phys. Rev. E* **2007**, *75*, 051403.

[22] B. P. Holownia, *Rubber Chem. Technol.* **1975**, *48*, 246.

[23] R. M. Christensen, in *Mechanics of Composite Materials*, Dover Publications, Mineola **2005**, pp. 31–72.

[24] R. M. Christensen, in *Mechanics of Composite Materials*, Dover Publications, Mineola **2005**, pp. 73–105.

[25] Z. Laufer, Y. Diamant, M. Gill, G. Fortuna, *Int. J. Polym. Mater.* **1978**, *6*, 159.

[26] G. R. Liu, *Compos. Struct.* **1998**, *40*, 313.

[27] K. M. Kalayeh, A. Charalambides, S. Bergbreiter, P. G. Charalambides, *IEEE Sens. J.* **2017**, *17*, 274.

[28] K. M. Kalayeh, P. G. Charalambides, *Sensors* **2018**, *18*, 3614.

[29] R. H. Pritchard, P. Lava, D. Debruyne, E. M. Terentjev, *Soft Matter* **2013**, *9*, 6037.

[30] Y. Jiang, Z. Liu, N. Matsuhisa, D. Qi, W. R. Leow, H. Yang, J. Yu, G. Chen, Y. Liu, C. Wan, Z. Z. Z. Liu, X. Chen, *Adv. Mater.* **2018**, *30*, 1706589.

[31] M. Sudheer, P. K. R, S. Somayaji, *Am. J. Mater. Sci.* **2015**, *5*, 162.

[32] K. K. Chawla, in *Composite Materials*, Springer, New York **2012**, pp. 337–386.

[33] J. C. Halpin, J. L. Kardos, *Polym. Eng. Sci.* **1976**, *16*, 344.

[34] E. Porte, T. Sipple, L. Sanchez Botero, D. Shah, R. Kramer-Bottiglio, *IEEE Int. Conf. Soft Robot.* **2021**, 412.

[35] R. A. Bilodeau, M. C. Yuen, R. Kramer-Bottiglio, *Adv. Mater. Technol.* **2019**, *4*, 1900276.

[36] F. López Jiménez, S. Pellegrino, *Int. J. Solids Struct.* **2012**, *49*, 635.

[37] M. Omidi, H. Rokni, A. S. Milani, R. J. Seethaler, R. Arasteh, *Carbon* **2010**, *48*, 3218.

[38] B. Liu, X. Feng, S. M. Zhang, *Compos. Sci. Technol.* **2009**, *69*, 2198.